Acoustic Warfare: Bubble Clouds

H. Levine

October 1992

JSR-91-113

Approved for public release; distribution unlimited.

JASON
The MITRE Corporation
7525 Colshire Drive
McLean, Virginia 22102-3481
(703) 883-6997

REPORT DOCUMENTATION PAGE

Form Approved OMB No. 0704-0188

1. AGENCY USE ONLY *(Leave blank)*

2. REPORT DATE
October 1, 1992

3. REPORT TYPE AND DATES COVERED

4. TITLE AND SUBTITLE
Acoustic Warfare: Bubble Clouds

5. FUNDING NUMBERS
PR - 8503A

6. AUTHOR(S)
H. Levine

7. PERFORMING ORGANIZATION NAME(S) AND ADDRESS(ES)
The MITRE Corporation
JASON Program Office A20
7525 Colshire Drive
McLean, VA 22102

8. PERFORMING ORGANIZATION REPORT NUMBER
JSR-91-113

9. SPONSORING/MONITORING AGENCY NAME(S) AND ADDRESS(ES)
Defense Advanced Research Projects Agency
3701 North Fairfax Drive
Arlington, Virginia 22203-1714

10. SPONSORING/MONITORING AGENCY REPORT NUMBER
JSR-91-113

11. SUPPLEMENTARY NOTES

12a. DISTRIBUTION/AVAILABILITY STATEMENT
Approved for public release. Distribution unlimited.

12b. DISTRIBUTION CODE

13. ABSTRACT *(Maximum 200 words)*

In this report, we survey the basic ingredients that go into the bubble cloud hypothesis for the enhanced acoustic backscatter seen at high enough frequency and wind speed. The basic picture that has been proposed is that spilling waves generate foamy water which is then subducted downward, modifying the local sound velocity. One proposed mechanism for the downwelling current necessary to accomplish the required subduction is the Langmuir circulation cell; we will see that this is sufficient but other mechanisms may also contribute. Our dicsussion naturally breaks up into the hydrodynamics issues related to bubble generation and subduction and to acoustic issues related to scattering from a given distribution of air density below the surface.

14. SUBJECT TERMS
acoustic backscatter, bubble clouds, Laplace Green, langmuir circulations

15. NUMBER OF PAGES

16. PRICE CODE

17. SECURITY CLASSIFICATION OF REPORT	18. SECURITY CLASSIFICATION OF THIS PAGE	19. SECURITY CLASSIFICATION OF ABSTRACT	20. LIMITATION OF ABSTRACT
UNCLASSIFIED	UNCLASSIFIED	UNCLASSIFIED	SAR

1 BUBBLE CLOUDS

In this report, we survey the basic ingredients that go into the bubble cloud hypothesis for the enhanced acoustic backscatter seen at high enough frequency and wind speed. The basic picture that has been proposed is that spilling waves generate foamy water which is then subducted downward, modifying the local sound velocity. One proposed mechanism for the downwelling current necessary to accomplish the required subduction is the Langmuir circulation cell; we will see that this is sufficient but other mechanisms may also contribute. Our discussion naturally breaks up into the hydrodynamics issues related to bubble generation and subduction and to acoustic issues related to scattering from a given distribution of air density below the surface.

1.1 Spilling Breakers

It is well known that as the amplitude of a gravity wave increases, the waveform develops a relatively sharp peak. If the peak slope gets too large, the wave will break. That is, the water will be unable to remain in a laminar state near the wave crest and turbulence will set in. There is a qualitative difference between a plunging breaker in which a double-valued nature of the crest is quite extreme and the more gentle spilling breaker in which the instability is confined to near the crest. This difference is clearly seen in Figure 1-1. There is a general expectation that spilling breakers are by far more the common type in the open ocean.

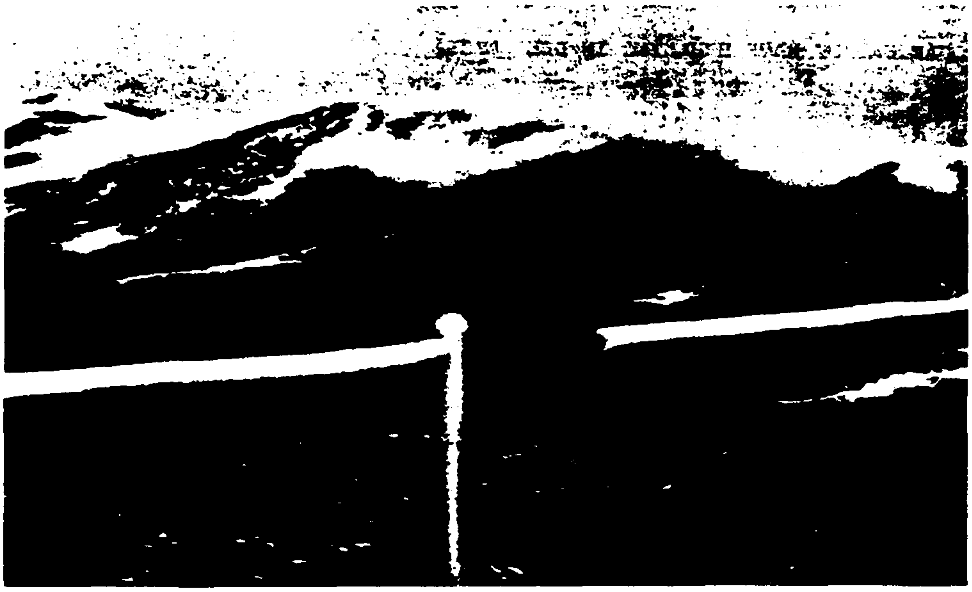

Figure 1-1a. Spilling breakers in the N. Atlantic, in wind force 6 (from Coles, 1967).

Figure 1-1b. A deep-water plunging breaker in the N. Atlantic (from Coles, 1967).

An estimate of the wave steepness at which breaking will occur can be obtained by considering the limiting wave amplitude/wavelength ratio. To do this, we can use a boundary integral method to find steady-state gravity waves. If we consider two-dimensional inviscid flow, we can represent the velocity as

$$\vec{v} = \vec{\nabla} \times \hat{z}\Psi(x, y)$$

where Ψ is the streamfunction, $\hat{x}$ represents a horizontal direction and $\hat{y}$ the vertical. Since $\vec{\nabla} \times \vec{v} = 0$, we have

$$\nabla^2\Psi = 0$$

the only source for Ψ is at the wave surface, due to the fact that the tangential velocity v_t (and hence the normal derivative of the streamfunction) is discontinuous at the fluid-air interface. We can therefore write

$$\Psi = \int G v_t \, ds'$$

where G is the Laplace Green's function. If we use an assumed periodicity of $\lambda = 2\pi$ to define a length scale, the proper Green's function is [Kessler, Koplik and Levine, 1988]

$$G_0 = -\frac{1}{4\pi} \log\left(1 - 2\cos(x - x')e^{-|y-y'|} + e^{-2|y-y'|}\right)$$
$$-\frac{1}{2}(|y - y'| - (y - y'))$$

for infinite depth and

$$G = G_0 + \frac{1}{4\pi} \log\left(1 - 2\cos(x - x')e^{-|2H-y-y'|} + e^{-2|2H-y-y'|}\right)$$

for fluid of unperturbed depth H. To find v_t, we use Bernoulli's law

$$\tfrac{1}{2}\vec{v}^2 + gy + p/\rho = \tfrac{1}{2}B$$

where B is Bernoulli's constant. The air pressure can be taken to equal zero and the normal velocity equals zero in the moving frame of the wave. Hence $v_t^2 = B - 2gy$ (we are neglecting surface tension). We can rescale g to 1 by proper choice of time scale. The equation for the interface follows from substituting v_t in the integral equation and setting $\Psi = 0$ everywhere on the air-fluid interface. This equation must be supplemented by the area constraint (i.e. incompressibility).

$$\int y_s \, dx' = 0$$

and the wave phase speed c is determined by

$$\Psi \sim -cy \quad (y \to -\infty) \quad \text{(infinite depth)}$$

$$\Psi(y = -H) = -cH \quad \text{(finite depth)}\,.$$

To solve these equations, we parameterize the curve by a finite set of points equally spaced in arclength and iterate using Newton's algorithm. For small amplitude $a \equiv \max y - \min y$, the wave is purely sinusoidal. At slightly larger a, we recover the analytic formula found by Stokes

$$c^2 = \frac{g^2}{k}\,(1 + a^2 k^2)\,.$$

Finally, at $a \simeq .44$, we reach the wave of maximum height at which the solution branch ends (see Figure 1-2). This is sometimes referred to as the 120° Stokes solution. Any attempt to put more energy into this wave will invariably cause the wave to break. It has been pointed out by Banner and Phillips (1974) that surface wind drift may lower the steepness at which breaking sets in, at least for small scale waves.

The preceeding discussion has been for a fully periodic wavetrain. In the ocean, a more typical instance is the existence of wave groups which advance

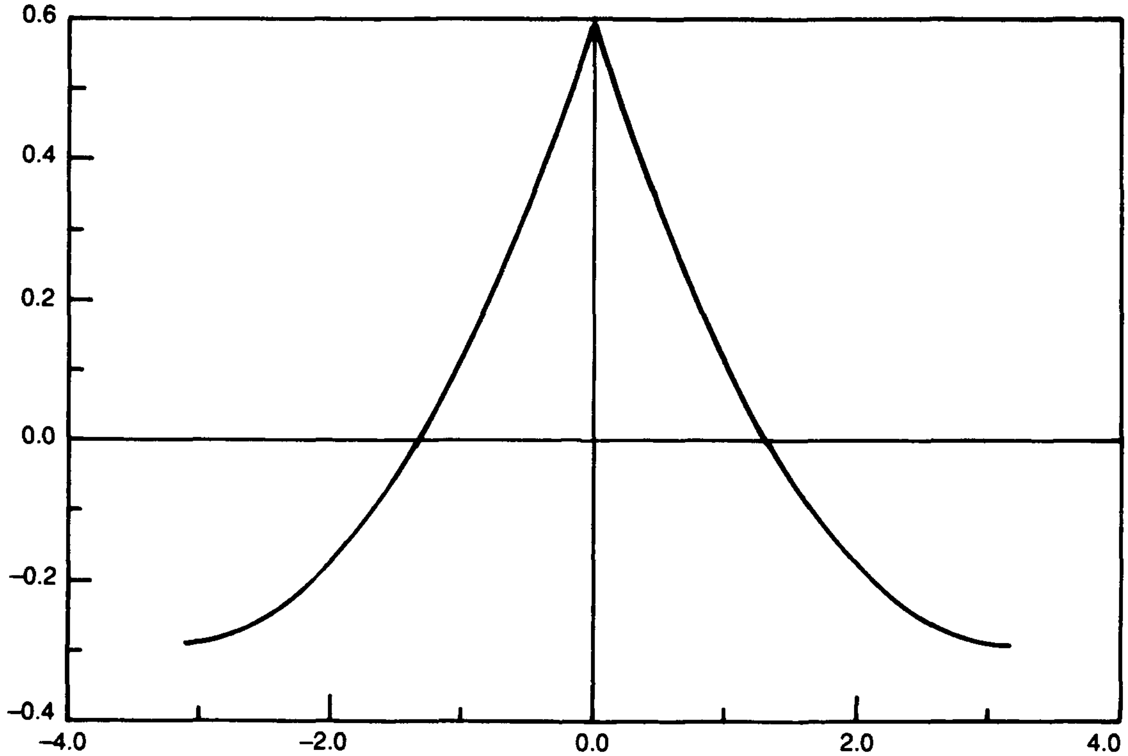

Figure 1-2. **Wave shape immediately before breaking (*ka* = .44).**

at the group velocity $V_g = \frac{1}{2}c$. Since this is smaller than the phase speed, individual waves inside the group advance through it, grow in amplitude and then subside. If the amplitude at the group center becomes of order of the aforementioned maximal amplitude, breaking will occur. As pointed out by Donelan, Longuet-Higgins and Turner (1972), this process is approximately periodic in time with period equal to twice the wave period. This offers an explanation for some anectodal evidence regarding the periodic appearance of whitecaps, with a periodicity that depends on the wave speed. If verified, a tendency for periodic repeats of bubble generation with a rate determined by the measurable surface waves (whose velocity is given by the Doppler shift of the Bragg scattering) could be a useful discrimination method.

Given that breaking is determined by having the waves grow to a maximal amplitude, the percentage of the ocean surface covered by whitecaps should depend both on the wind velocity U (measured at, say, 10 meters height) and the fetch (Monahan and Monahan, 1985). The latter dependence has not always been looked at explicitly; in most of the early literature on phenomenological fits to whitecap coverage, the assumed dependence was taken to be (see Monahan and O'Muircheartagh, 1986)

$$w = BU^{\alpha},$$

with U in m/sec. This led to estimates of $\alpha \simeq 3.4$ with B around 3.8×10^{-6}. Little systematic dependence on atmospheric stability has been observed. Perhaps the most sophisticated treatment of the phenomenology, discussed in Monahan and O'Muircheartagh, predicts the comprehensive formula $w \equiv w(U, \Delta T, T_w, d, F)$ where $\Delta T \equiv T_{\text{water}} - T_{\text{air}}$ is related to the atmospheric stability, T_w is the actual water temperature, F is the fetch and d is the wind duration.

The basic model of the spilling breaker itself is due to Longuet-Higgins and Turner (1974). A cartoon picture of the flow is given in Figure 1-3a. The basic idea is that the turbulent water is treated as a distinct fluid which slides down the forward face of the large amplitude wave. This fluid is less dense than the underlying "laminar" fluid since the turbulent flow incorporates air bubbles — typical estimates of the density of such self-aerated flows suggest that the density on a 30° slope might be from 70% to 90% that of pure water. This flow is complicated by the shear between the falling turbulent flow and the rising (in the frame moving with the wave) laminar basement; this shear presumedly tends to inject water into the turbulent layer and also retards the motion via friction. As the wave amplitude subsides, the gravity impact forcing driving the turbulent flow downward decreases and the foam is carried over the top to the back face. The slope at which this occurs is in some ways similar to the angle of repose for granular flows at which an avalanche will be suppressed (as we go to $\theta < \theta_R$) by the shear friction with the underlying solid ground. A picture of the entire sequence, taken from Donelan and Pierson (1987) is given in Figure 1-3b.

It is fair to say that the problem of predicting the flows, air densities, and eventually bubble sizes and number distribution in a spilling breaker is far from being solved. However, it is probably a reasonable guess that the typical spilling event and the frequency of occurence depends most strongly on the wind and on the fetch.

1.2 Langmuir Circulations

Foamy water can only scatter underwater sound effectively if certain

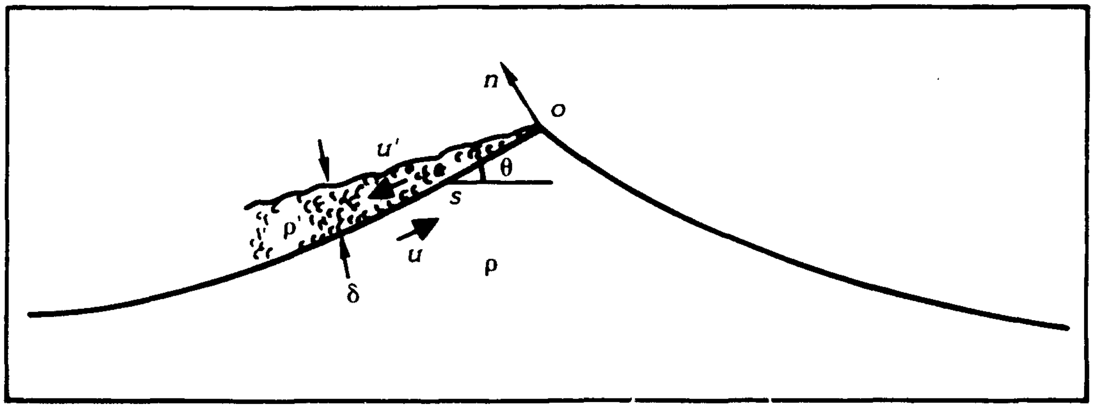

Figure 1-3a. Sketch showing the features of a spilling breaker which are incorporated in the theoretical model. The wave is moving from the right to left and has a whitecap on its forward face. The velocities in both the wave and whitecap are measured relative to the wave crest, with positive direction downwards.

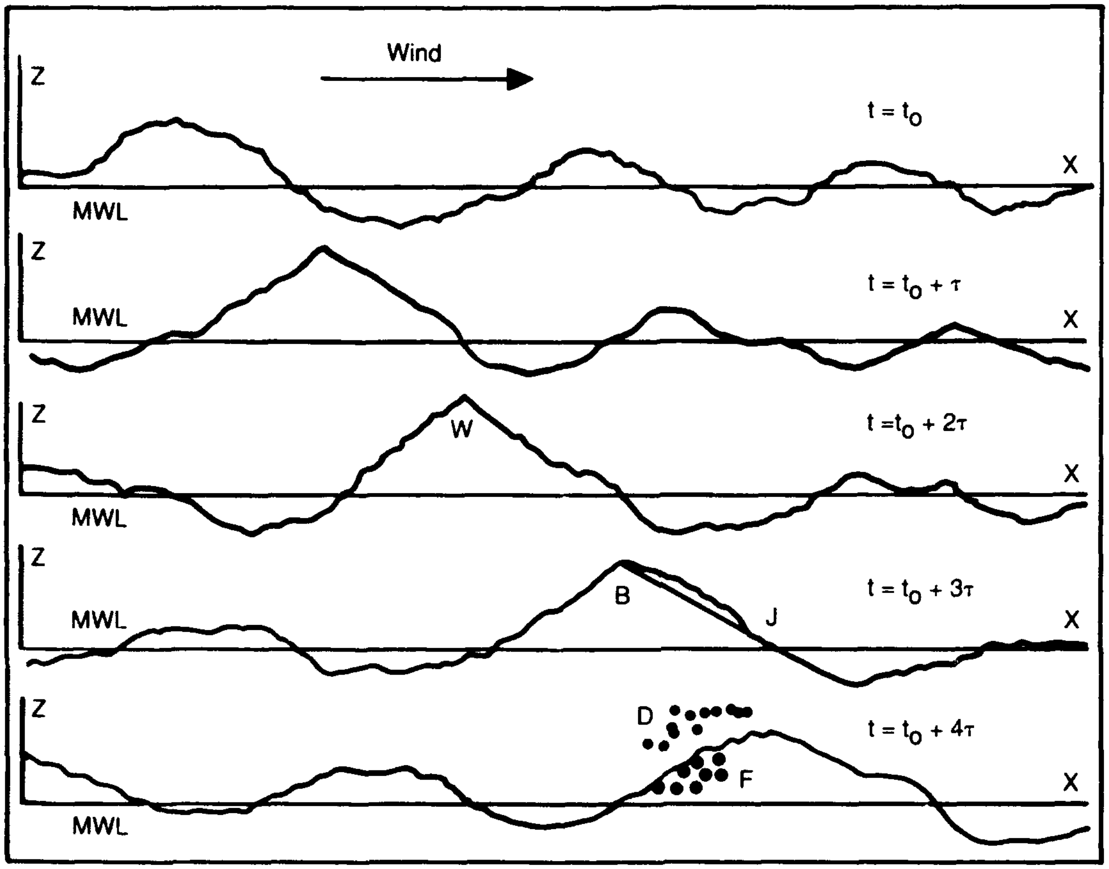

Figure 1-3b. Schematic diagram, with the vertical scale exaggerated, through the center line of a group of waves. As the wave on the 'eft at the top advances from $t = t_0$ to $t = t_0 + \tau$, it steepens and forms a sharp we..ge (labeled W) at $t = t_0 + 2\tau$. This is followed for a short while by a spilling breaker (b), with a hydraulic jump (J) at the toe of the breaker, as at $t = t_0 + 3\tau$. As the wave decreases in height on progressing through the group, the action ceases and a foam patch (F) and water drops (D) are left behind.

conditions are met. First, there must be significant air density at depths removed from the air/water interface which acts as a pressure release boundary. Secondly there must be some non-trivial horizontal structure to the bubble density profile. A uniform layer of aerated water will just present a lower "effective" surface and have no appreciable backscatter.

A typical phenomenological assumption for the onset of acoustic backscatter is $fU^2 > 10^4$ where f is the frequency in Hz and U the windspeed in m/sec. Early estimates of how far down bubbles would be expected to be observed came up with the conclusion that the bubble hypothesis could not account for the increased backscatter; roughly, if one believes that a significant backscatter can occur at low frequencies ($f \sim 100$Hz) for $U > 10$ m/sec, this requires bubble cloud protrusions of order 5-10 meters below the effective pressure release surface. A 100 μ size bubble, assumed to suffer low Reynolds number Stokes drag, will have a rise velocity of 2.2 cm/sec: clearly, we must have a vertical downwelling of sufficient magnitude and for sufficient duration that within a bubble lifetime, bubbles are indeed advected 10 meters downward. For bubbles that start out at, say 100 μ, an estimate for the dissolution time is (see JASON report JSR-87-101)

$$\left(\frac{r_0}{10\mu m}\right)\left(\frac{1\mathrm{m}}{\mathrm{depth}}\right) \cdot 23\,\mathrm{seconds}$$

$\simeq$1 minute at 5 meters. (Small bubbles have shorter dissolution lifetimes but a smaller rise velocity compensates to some extent.) For the required penetration, we thus might require

$$(v_d - 2.2\ \mathrm{cm/sec}) \simeq \frac{5-10\,\mathrm{meters}}{(60)(2.5\,\mathrm{minutes})}$$

which means a downwelling of perhaps 10 cm/sec. See Thorpe (1982) for a more comprehensive discussion leading to a similar conclusion.

The leading candidate for providing the necessary downwelling is the Langmuir circulation cell. (There may also be occasional downdrafts due to sudden cooling giving rise to a convective instability, but these seem to be rare.) These cells are associated with oft observed windrows, long parallel streaks in the wind direction caused by convergence zones at the surface current. It has been noted by Thorpe and Hall (1982) that waves break with equal frequency in windrows and between them (i.e. there is no statistical correlation between Langmuir circulation patterns and wave breaking) and so the wave breaking can be thought of as providing a uniformly distributed source for the Langmuir current. Assuming that we have some empirical understanding of the rate of foam generation (and perhaps an idea of the bubble size distribution if there is no one specific "typical" size), we merely need to understand the causes of, and patterns in, typical circulation cells. Unfortunately, this has proven quite difficult.

Before continuing our discussion, we would like to emphasize that to date there is no definitive proof that Langmuir cells are necessary. It is conceivable the wave breaking by itself may under some conditions push enough macrobubbles downward to affect acoustic backscatter, at least at somewhat higher frequencies. Our goal is to outline one self-consistent picture of what could be happening, with much additional effort needed to confirm or invalidate this scenario.

A review of the possible causes of Langmuir circulations was presented by Leibovich (1983), with more recent measurements by Weller *et al.* (1985) and Smith (1991). A schematic picture of a typical flow is presented in Figure 1-4; the typical flow velocities are 5-10 cm/sec (Figure 1-5a), and typical spacing and depths believed to be connected to the mixed layer depth can range from several meters to several hundred meters. For the typical

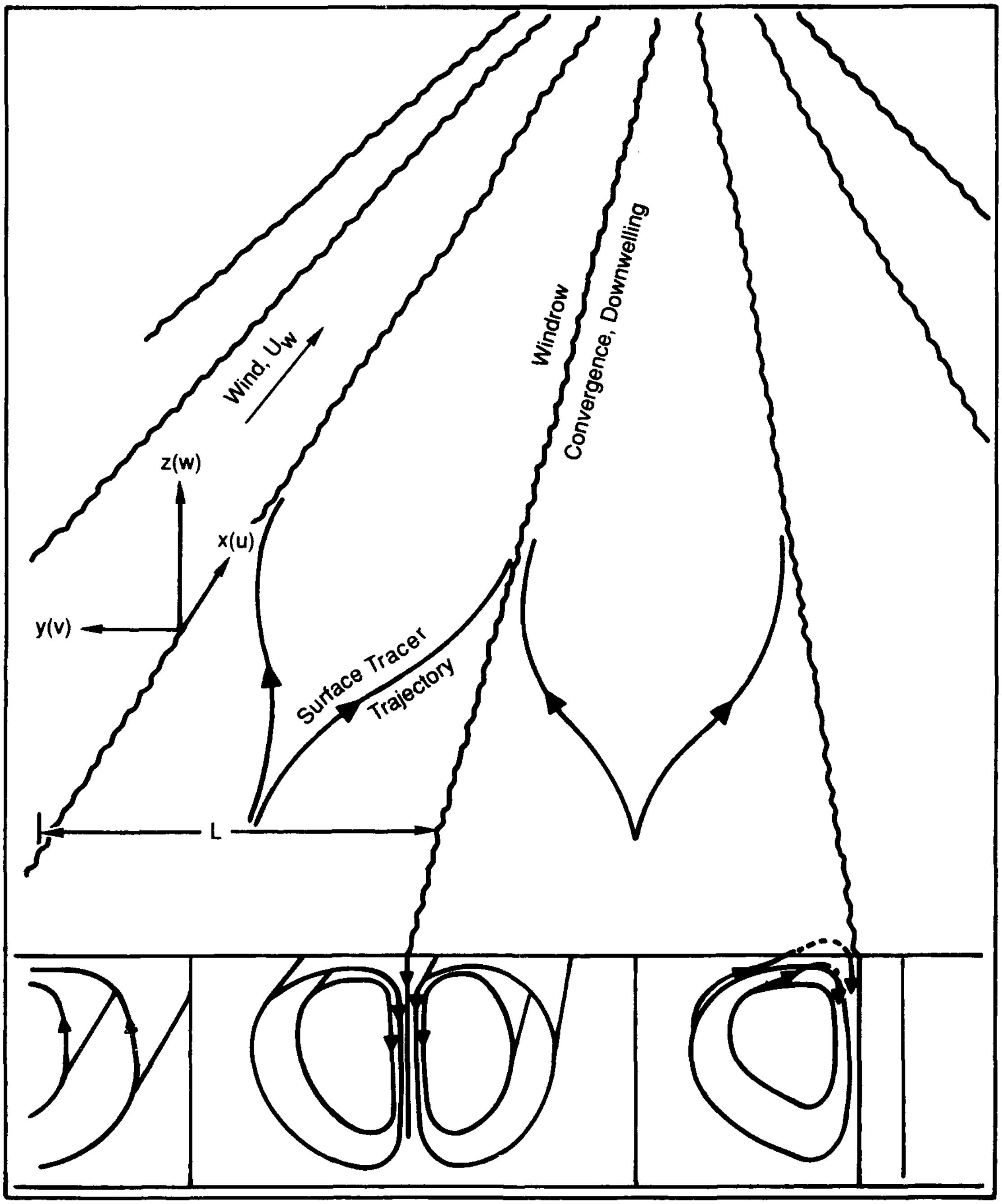

Figure 1-4. Illustration of Langmuir circulations showing surface and subsurface motions (from Leibovich, 1983).

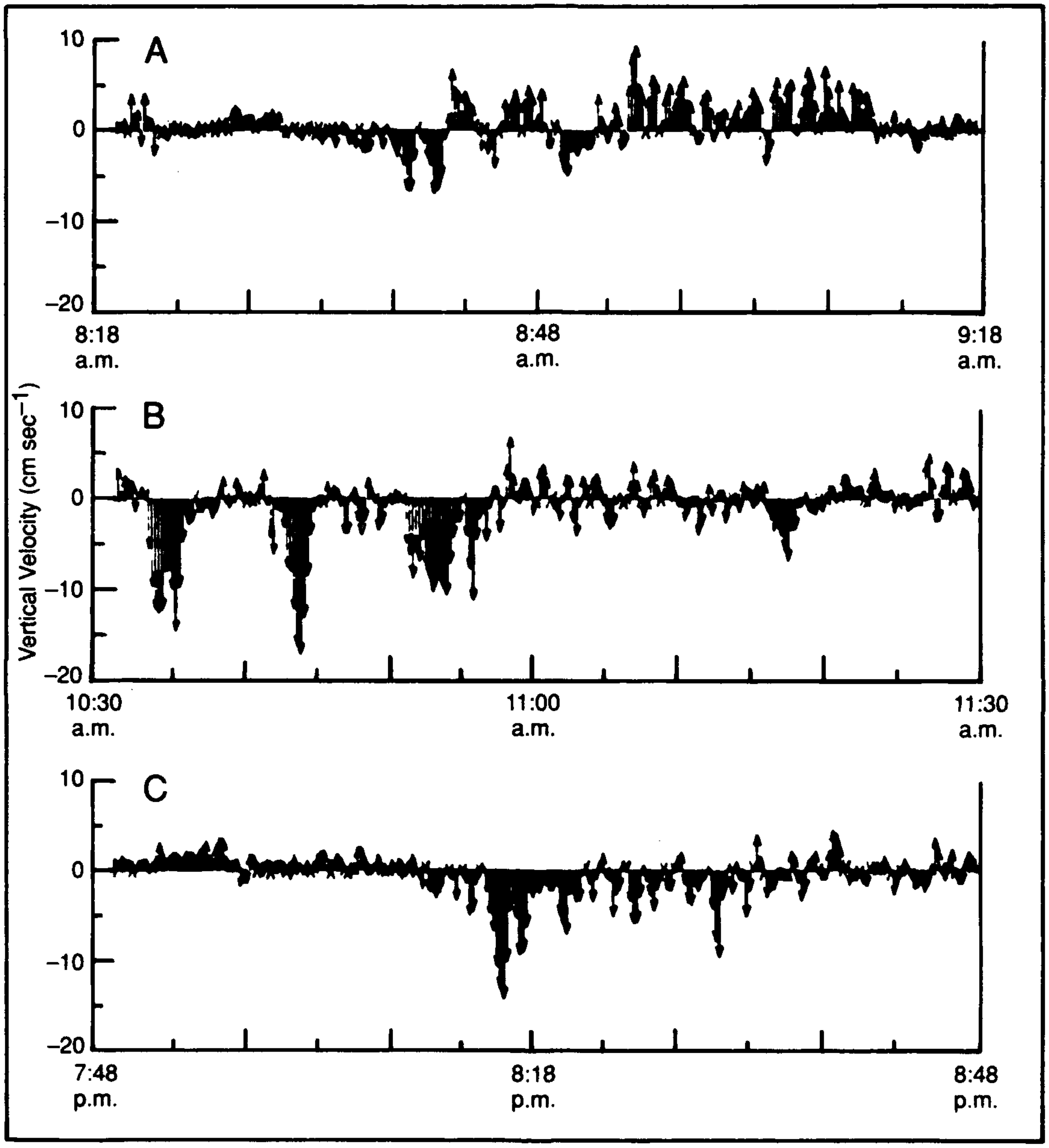

Figure 1-5a. Three time series of vertical velocity from 13 December.

sonar of interest in active acoustics, returns from bubble clouds in individual descending curtains will probably not be resolved and one will instead see a composite return.

A theoretical model which adequately describes the observations of oceanic Langmuir cells is still lacking. The most likely explanation seems to be that of a Stokes drift (caused by waves) interacting with an initially horizontally uniform current (but vertically varying) u_c. In the basic hydrodynamic equations of motion, there is a term of the form

$$\begin{aligned} \vec{f} &= \vec{u}_s \times (\vec{\nabla} \times \vec{u}_c) \\ &= \hat{y} u_s \frac{\partial u_c}{\partial y} \end{aligned}$$

if both the Stokes drift and the current shear are in the wind direction (say $\hat{x}$). This is like a gravitational force, pointing downward since $\frac{\partial u_c}{\partial y} < 0$; it of course can be statically balanced by a pressure gradient. If however the gradient of this force is positive, the ocean will behave like an unstably stratified fluid and begin to convect via instability growth.

Now u_s is determined by the square of the wave amplitude a times the characteristic wave frequency σ, whereas the current shear will be determined by wind stress to be u_*^2/ν_T, where ν_T is some effective kinematic viscosity and u_* is a friction velocity. Via dimensional analysis, one can predict a dimensionless Langmuir number

$$La \sim \left(\frac{\nu_T^3 k^2}{\sigma u_*^2 a^2} \right)^{1/2}$$

(k is the wavenumber) which governs the onset of the instability once dissipation is taken into account. Stratification of the fluid will, of course, tend to reduce the instability and gives rise to the notion mentioned above that the cells only extend downward within the mixed layer. Typical windspeeds for the onset of circulation range around 10 m/sec. The growth of a Langmuir cell in an ocean experiment after the wind increased from 8 to 13 m/sec is shown in Figure 1-5b. There is no obvious explanation for the time dependence of the wave vector in this data.

Most of the measurements of Langmuir circulations have been accomplished by high frequency sonar scattering from below the surface (actually scattering from the bubbles!) (see Figure 1-5). We would like to mention the possibility of using the SAR interferometry technique (Goldstein, Barnett and Zebker, 1989) of possibly being capable of resolving the surface circulation pattern of large Langmuir cells. The SAR imaging resolution scale is limited mostly by velocity bunching by the ambient surface waves. This "bunching" is due to the mistaken assignment of position by the SAR algorithm due to the motion at the sea surface. Under moderate sea states one might have a velocity variance $\langle v^2 \rangle \sim (50\text{cm/sec})^2$ which translates, at say 5 km range, 100 m/sec, to a resolution

$$(.50)\,\frac{5 \times 10^3}{100} \simeq 25\,\text{meters}.$$

The interferometric technique consists of two SAR antennas spaced apart by a short distance, and the velocity of the surface current is found by comparing the images of the two synthetic apertures. The claimed velocity resolution in a recent experiment was 5-10 cm/sec, roughly the same order as the circulation currents which have the further virtue of being roughly spatially periodic and therefore easy to spot by looking at peaks in the (spatial) Fourier transform.

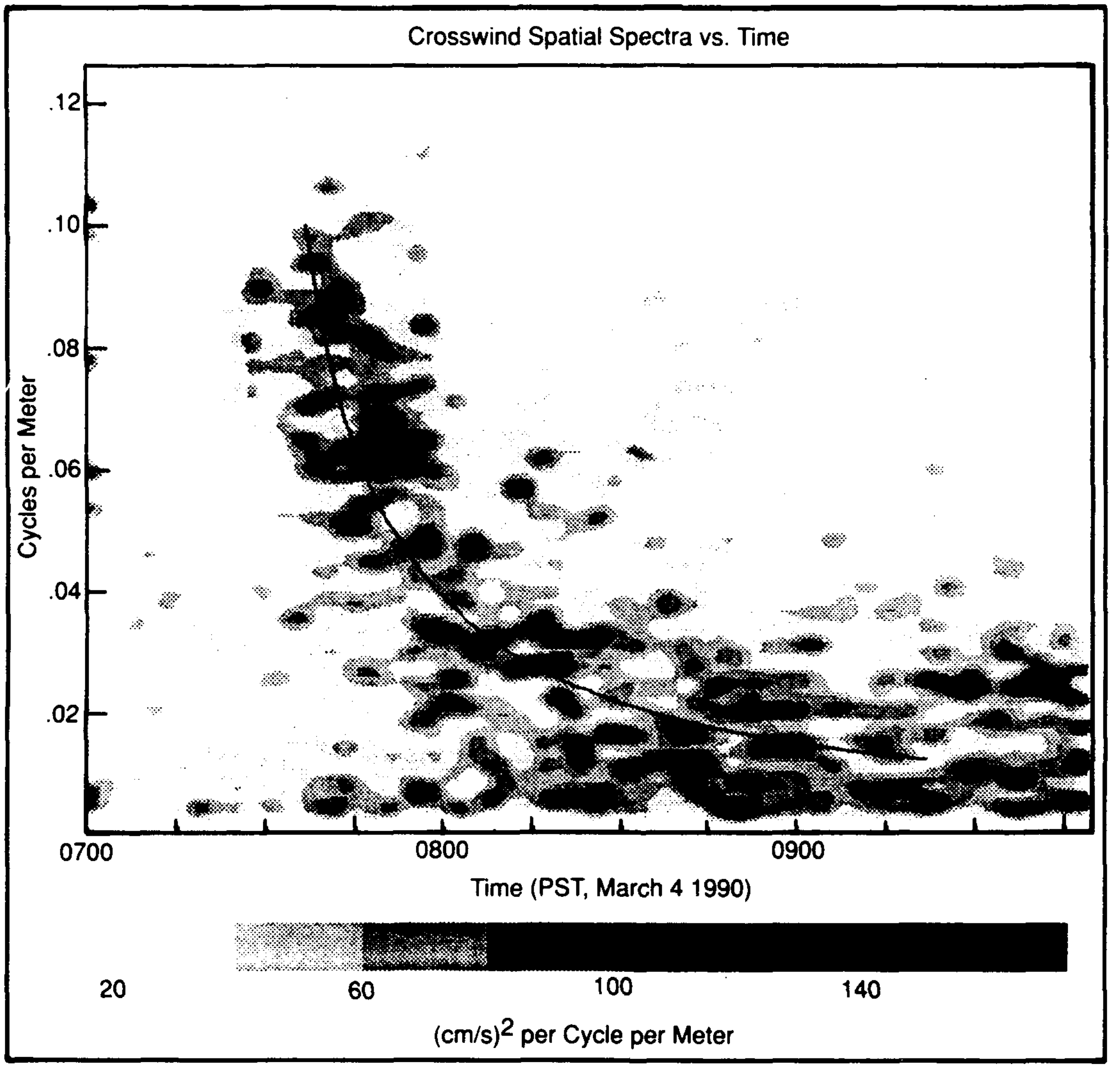

Figure 1-5b. Growth of Langmuir cell size. Solid line is 40 m/hr growth rate (from Smith, submitted 1991): wind increases from 8 m/sec to 13 m/sec at 7:20 A.M.

1.3 Acoustic Scattering

The story so far has been that spilling breakers act as a source for foamy water which occasionally is advected downward to depths of 5 to 10 meters by Langmuir circulation cells. As far as the acoustic problem is concerned, what we really need is a plot of air density as a function of depth and horizontal position. This is true if we are scattering from clouds of bubbles as macroscopic regions with changed acoustic velocities, as distinct from any resonant contributions associated with "macro-bubbles". Since this seems for the moment to be the most likely hypothesis, we will limit our discussion to this case.

Measurements of bubble density as a function of depth is again accomplished by high frequency sonar. A review of a typical experimental setup and typical results is given by Thorpe (1986). In Figure 1-6a we reproduce the results of a vertical ranging sonar showing typical bubble plumes as a function of time; in Figure 1-6b, a sidescan sonar records the horizontal structure showing the connection between wavebreaking events and bubble plume formation. In this study, evidence of bubble bands were found above wind speeds of 7 m/sec, roughly consistent with the expected onset of Langmuir circulations. Somewhat surprisingly, the typical spacing between bands is only of order 5 m, much shorter than the typical large cell size. This might be evidence of more complex circulation patterns (nested cells, e.g.) or of the incompleteness of the Langmuir cell explanation. Soon after initial formation, the bubbles quickly lost any velocity imparted by the wave and were merely advected by oceanic currents.

In a similar experiment, Farmer and Vagle (1989) have measured the

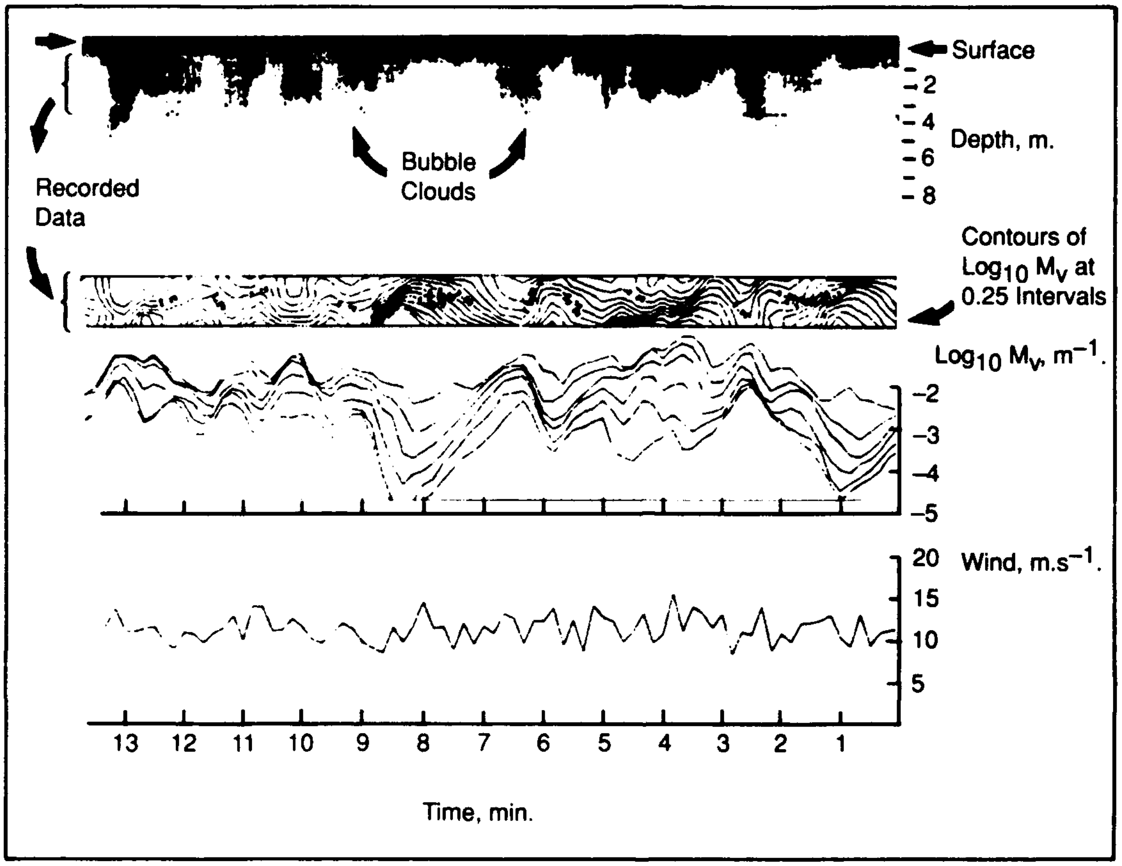

Figure 1-6a. Bubbles observed using a vertically pointing sonar. The sonograph (top) shows clouds of bubbles below the surface. Below this are contours of log M_v and plots of M_v measured at six levels in the depth range bracketed at the left of the sonograph. The wind speed is shown at the bottom. The wind direction was southwesterly, the fetch exceeding 10 km, and the air temperature was 1.75K below the water temperature.

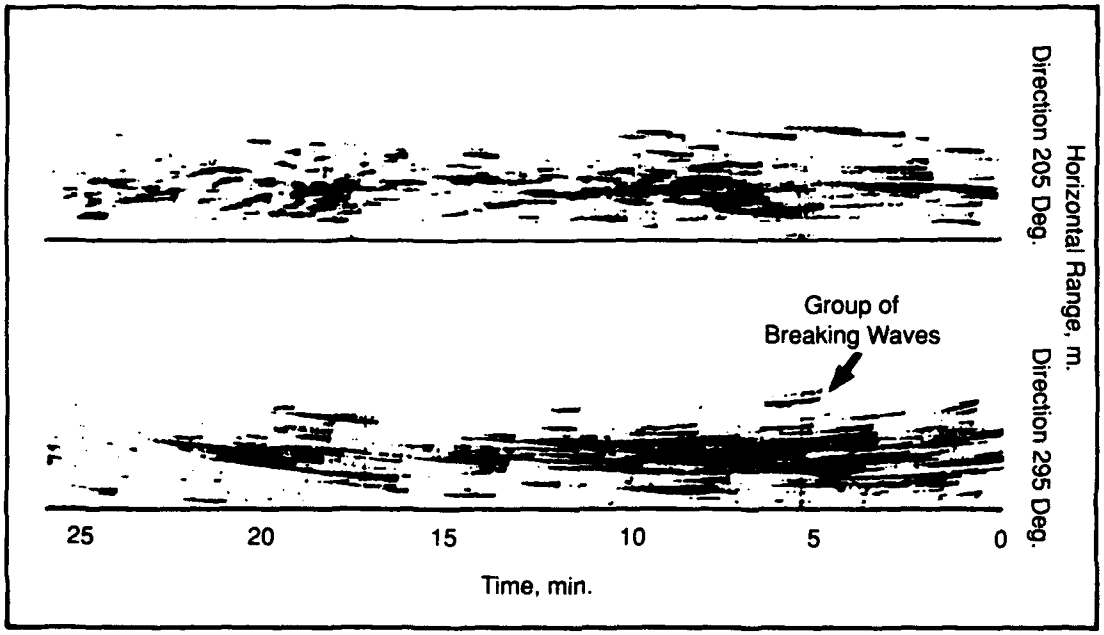

Figure 1-6b. Sonograph from side-scan sonar. The range is measured along the surface from a position immediately above the sonar. The near-horizontal streaks are due to sound reflected from bubble clouds. The wind was 6.5ms^{-1}, westerly. Groups of breaking waves can be seen approaching the sonar down the beam in the 295 degree direction.

air volume fraction as a function of depth; their graph is reproduced here in Figure 1-7a. Although the volume fraction is quite small, the effect on sound speed, given via the index of refraction

$$n^2 = 1 + \frac{23,000\phi}{1 + z/10\,\text{meter}}$$

$$\phi = \text{air volume fraction}$$

is still capable of causing scattering. If, following Henyey (1991), we model bubble clouds as cylinders with typical radii of 1-2 meters, this depth distribution can be converted to an area distribution for plumes as a function of depth (Figure 1-7b). The prediction of large plumes every 1500 m^2 means that for cells of size 100 m, there is a peak downwelling (or perhaps a wave breaking that more effectively inserts foamy water into the downwelling flow) every 15 m or so along the windrows. More careful sonar measurements should be able to selectively search for large plumes (by the necessary range gating in a vertical system) to see if this is at all reasonable.

Given bubble plumes determined in the above manner from the measured volume fraction data, Henyey (1991) has given a convincing demonstration that the enhanced backscatter (i.e., the Chapman-Harris (1962) curve) could be accounted for. In some sense, the acoustic calculation is by far the easiest piece of the puzzle; with the exception of very shallow grazing angle, multiple scattering effects are negligible and more exotic phenomena (such as localization due to repeated interactions with plumes) highly unlikely.

In some more recent work, Henyey (private communication) has pointed out that some new data suggests that the bubble cylinder radii may actually be somewhat larger than the 1-2 meters originally chosen. Again, various realistic choices of larger cylinders still give fairly consistent answers. One should note that there has been no reported evidence of strong asymmetry of

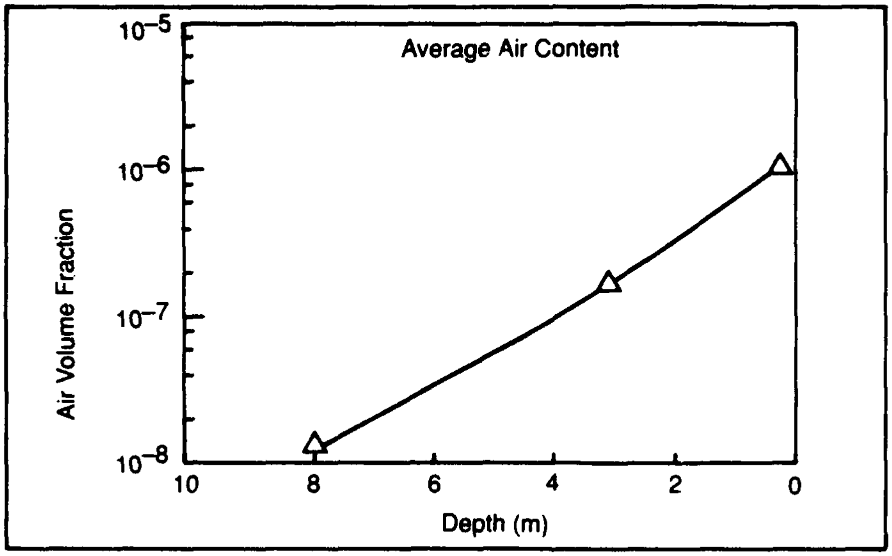

Figure 1-7a. Air volume fraction from the Fasinex experiment, extracted from the results of Farmer and Vagle (1989). This data constrains the microbubble plume model at a wind speed of 12 m/s.

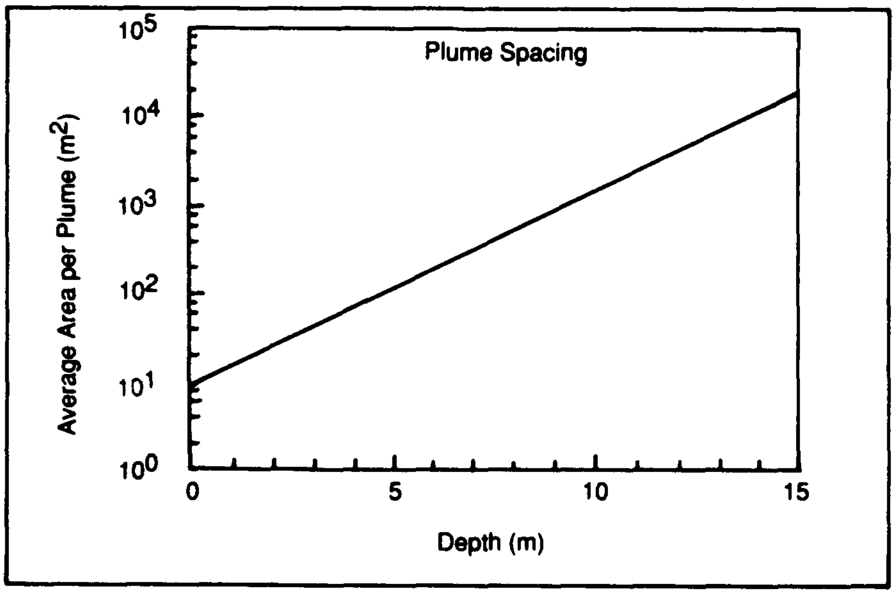

Figure 1-7b. Model prediction for the plume specing. An experiment which can resolve 5-m plumes should have a resolution cell no longer then $10^2 m^2$.

should note that there has been no reported evidence of strong asymmetry of the backscatter; this is consistent with scattering from rare, isolated plumes but would possibly contradict a scattering mechanism based on a continuous enhancement of air volume fraction all along a Langmuir downwelling curtain. At the present level of sophistication, all one can really say is that physically reasonable choices of clouds of microbubbles consistent with sonar measurements can account for the enhanced backscatter.

One aspect of the current multi-step approach to explaining the acoustic response is the possible sensitivity of the result to an almost endless set of environmental issues. To briefly recap, whitecap coverage will depend mostly on wind speed, but also on fetch and on air and sea temperatures. Langmuir circulation patterns can depend on swell (which causes Stokes currents) and depth of the mixed layer, in addition to wind and wind direction. Any experimental efforts to study acoustic scattering must be cognizant of the need to carefully determine these controlling parameters.

REFERENCES

1. D. Kessler, J. Koplik and H. Levine, *Adv. in Phys.* **37**, 255 (1988).
2. M.L. Banner and O.M. Phillips, *J. Fluid Mech.* **65**, 647 (1974).
3. R. Chapman and J. Harris, *J. Acoust. Soc. America* **34**, 1592 (1962).
4. K.A. Coles, "Heavy weather sailing", London Adlard-Coles Ltd (1967).
5. M. Donelan, M.S. Longuet-Higgins and J.S. Turner, *Nature* **239**, 449 (1972).
6. M.A. Donelan and W.J. Pierson, *J. Geophy. Res.* **92**, 4971 (1987).
7. D. Farmer and S. Vagle, *J. Acoust. Soc. America* **86**, 1897 (1989).
8. R.M. Goldstein, T.P. Barnett and H.A. Zebker, *Science* **246**, 1282 (1989).
9. F.S. Henyey, *J. Acoust. Soc. America* **90**, 399 (1991).
10. S. Leibovich, *Ann Rev. Fluid Mech.* **13**, 391 (1983).
11. M.S. Longuet-Higgins, "Mechanisms of Wave Breaking in Deep Water" in *Sea Surface Sound*, B.R. Kerman, ed., Kluwer (1988).
12. M.S. Longuet-Higgins and J.S. Turner, *J. Fluid Mech.* **63**, 1 (1974).
13. E.C. Monahan and F. Monahan, "The Influence of Fetch on Whitecap Coverage", in "Oceanic Whitecaps and Their Role in the Air-Sea Exchange Process" E.C. Monahan and G. MacNiocaill (Reidel, 1985).
14. E.C. Monahan and I.G. O'Muircheartargh, *Int. J. Remote Sensing* **7**, 627 (1986).

15. I.S. Robinson, "Satellite Oceanography" Wiley (1985).

16. J.A. Smith, "Observed Growth of Langmuir Circulation", *J. Geophys. Res.*, submitted (1991).

17. S. Thorpe, *Phil. Trans. Roy. Soc. London* **A304**, 155 (1982).

18. S.A. Thorpe, "Bubble Clouds, A Review of Their Detection by Sonar" in "Oceanic Whitecaps and Their Role in the Air-Sea Exchange Process" E.C. Monahan and G. MacNiocaill (Reidel, 1985).

19. S.A. Thorpe and A.J. Hall, *J. Fluid Mech.* **114**, 237 (1982).

20. R. Weller, J. Dean, J. Marra, E. Francis and D. Boardman, *Science*, **227**, 1552 (1985).

DISTRIBUTION LIST

CMDR & Program Executive Officer
U S ArmyY/CSSD-ZA
Strategic Defense Command
PO Box 15280
Arlington, VA 22215-0150

Mr John Bachkosky
Deputy DDR&E
The Pentagon
Room 3E114
Washington, DC 20301

Dr Joseph Ball
Central Intelligence Agency
Washington, DC 20505

Dr Arthur E Bisson
DASWD (OASN/RD&A)
The Pentagon
ROOM 5C675
Washington, DC 20350-1000

Dr Albert Brandenstein
Chief Scientist
Office of Nat'l Drug Control Policy
Executive Office of the President
WASHINGTON DC 20500

Mr Edward Brown
Assistant Director
DARPA/NMRO
3701 North Fairfax Drive
Argonne, VA 22203-1714

Dr H Lee Buchanan, I I I
Director
DARPA/DSO
3701 North Fairfax Drive
Arlington, VA 22203-1714

Dr Curtis G Callan Jr
Physics Department
PO Box 708
Princeton University
Princeton, NJ 08544

Dr Ferdinand N Cirillo Jr
Central Intelligence Agency
Washington, DC 20505

Brig Gen Stephen P Condon
Deputy Assistant Secretary
Management Policy &
Program Integration
The Pentagon, Room 4E969
Washington, DC 20330-1000

Ambassador Herny F Cooper
Director/SDIO-D
Room 1E1081
The Pentagon
Washington, DC 20301-7100

D A R P A Library
3701 North Fairfax Drive
Arlington, VA 22209-2308

D T I C [2]
Cameron Station
Alexandria, VA 22314

Mr John Darrah
Senior Scientist and Technical Advisor
HQAF SPACOM/CN
Peterson AFB, CO 80914-5001

Dr Gary L Denman
Director
DARPA/DIRO
3701 North Fairfax Drive
Arlington, VA 22203-1714

DISTRIBUTION LIST

Dr Nancy Dowdy
USACDA
320 21st Street NW
Washington, DC 20451

Mr John N Entzminger
Chief Advance Technology
DARPA/DIRO
3701 North Fairfax Drive
Arlington, VA 22203-1714

Capt Kirk Evans
Director Undersea Warfare
Space & Naval Warfare Sys Cmd
Code PD-80
Department of the Navy
Washington, DC 20363-5100

Dr S William Gouse
Sr Vice President and
General Manager
The MITRE Corporation
Mail Stop Z605
7252 Colshire Drive
McLean, VA 22102

Mr Thomas H Handel
Office of Naval Intelligence
The Pentagon
Room 5D660
Washington, DC 20350-2000

Maj G Hard
Director of Space and SDI Programs
Code SAF/AQS
The Pentagon
Washington, DC 20330-1000

Dr Robert G Henderson
Director
JASON Program Office
The MITRE Corporation
7525 Colshire Drive
Mailstop Z561
McLean, VA 22102

Dr Barry Horowitz
President and Chief Exec Officer
The MITRE Corporation
202 Burlington Road
Bedford, MA 01730-1420

Dr William E Howard I I I [2]
Director for Space and Strategic Technolo
Office/Assistant Secretary of the Army
The Pentagon Room 3E474
Washington, DC 20310-0103

Dr Gerald J Iafrate
U S Army Research Office
PO Box 12211
4330 South Miami Boulevard
Research Triangle NC 27709-2211

J A S O N Library [5]
The MITRE Corporation
Mail Stop W002
7525 Colshire Drive
McLean, VA 22102

Dr George Jordy [25]
Director for Program Analysis
U S Department of Energy
ER30
OER
Washington, DC 20585

DISTRIBUTION LIST

Dr O' Dean P Judd
Los Alamos National Lab
Mail Stop A-110
Los Alamos, NM 87545

Dr Bobby R Junker
Office of Naval Research
Code 412
800 North Quincy Street
Arlington, VA 22217

Dr Herbert Levine
Department of Physics
Mayer Hall/B019
University of California/San Diego
La Jolla, CA 92093

Mr Robert Madden [2]
Department of Defense
National Security Agency
Attn R-9 (Mr. Madden)
Ft George G Meade, MD 20755-6000

Dr Arthur F Manfredi Jr [10]
OSWR
Central Intelligence Agency
Washington, DC 20505

Mr Joe Martin
Director
OUSD(A)/TWP/NW&M
Room 3D1048
The Pentagon
Washington, DC 20301

Mr James J Mattice
Deputy Assistant Secretary
SAF/AQ
Pentagon
Room 4D-977
Washington, DC 20330-1000

Mr Ronald Murphy
Director
DARPA/ASTO
3701 North Fairfax Drive
Arlington, VA 22203-1714

Dr Julian C Nall
Institute for Defense Analyses
1801 North Beauregard Street
Alexandria, VA 22311

Dr Gordon C Oehler
Central Intelligence Agency
Washington, DC 20505

Dr Peter G Pappas
Chief Scientist
U S Army Strategic Defense Command
PO Box 15280
Arlington, VA 22215-0280

Dr Ari Patrinos
Director
Environmental Sciences Division
ER74/GTN
US Department of Energy
Washington, DC 20585

Dr Bruce Pierce
USD(A)D S
Room 3D136
The Pentagon
Washington, DC 20301-3090

Mr John Rausch [2]
Division Head 06 Department
NAVOPINTCEN
4301 Suitland Road
Washington, DC 20390

DISTRIBUTION LIST

Records Resource
The MITRE Corporation
Mailstop W115
7525 Colshire Drive
McLean, VA 22102

Dr Fred E Saalfeld
Director
Office of Naval Research
800 North Quincy Street
Arlington, VA 22217-5000

Dr John Schuster
Technical Director of Submarine
and SSBN Security Program
Department of the Navy OP-02T
The Pentagon Room 4D534
Washington, DC 20350-2000

Dr Barbara Seiders [2]
Chief of Research
Office of Chief Science Advisor
Arms Control & Disarmament Agency
320 21st Street NW
Washington, DC 20451

Dr Philip A Selwyn [2]
Director
Office of Naval Technology
Room 907
800 North Quincy Street
Arlington, VA 22217-5000

Superintendent
Code 1424
Attn Documents Librarian
Naval Postgraduate School
Monterey, CA 93943

Dr George W Ullrich [3]
Deputy Director
Defense Nuclear Agency
6801 Telegraph Road
Alexandria, VA 22310

Ms Michelle Van Cleave
Asst Dir/National Security Affairs
Office/Science and Technology Policy
New Executive Office Building
17th and Pennsylvania Avenue
Washington, DC 20506

Mr Richard Vitali
Director of Corporate Laboratory
US Army Laboratory Command
2800 Powder Mill Road
Adelphi, MD 20783-1145

Dr Edward C Whitman
Dep Assistant Secretary of the Navy
C3I Electronic Warfare & Space
Department of the Navy
The Pentagon 4D745
Washington, DC 20350-5000

Mr Donald J Yockey
U/Secretary of Defense For Acquisition
The Pentagon Room 3E9333
Washington, DC 20301-3000

Dr Linda Zall
Central Intelligence Agency
Washington, DC 20505

Mr Charles A Zraket
Trustee
The MITRE Corporation
Mail Stop A130
202 Burlington Road
Bedford, MA 01730